Single-Virus Tracking Reveals a Spatial Receptor-Dependent Search Mechanism

Eli Rothenberg,[†‡]* Leonardo A. Sepúlveda,[§¶] Samuel O. Skinner,[†¶] Lanying Zeng,[†] Paul R. Selvin,[†‡§] and Ido Golding[†‡§¶]*

[†]Department of Physics, [‡]Center for the Physics of Living Cells, and [§]Center for Biophysics and Computational Biology, University of Illinois at Urbana-Champaign, Urbana, Illinois; and [¶]Verna and Marrs McLean Department of Biochemistry and Molecular Biology, Baylor College of Medicine, Houston, Texas

ABSTRACT Viral infection begins with the binding of a virus to a specific target on the surface of the host cell, followed by viral genome delivery into the host and a continuation of the infection process. Before binding occurs, the virus must first find its receptor by a process whose details are largely unknown. We applied high-resolution fluorescence microscopy and single-particle tracking to elucidate the target-finding process in bacteriophage λ as it infects an *Escherichia coli* cell. By monitoring the motion of individual viruses through the early stages of infection, we identified a unique spatial focusing process that allows a virus to arrive from its initial random landing site to its destination at the cell pole. The search process is governed by the interaction between the virus and the LamB receptors, and by the spatial organization of the receptor network on the cell surface. Our findings allowed us to develop a theoretical model for the target-finding process that reproduces the key features observed in experiment. We discuss the possible implications of our findings for the process of viral receptor-finding in higher systems.

INTRODUCTION

The details of early virus-host interaction vary greatly among different systems (1–4), but in all cases the viral-host binding process involves a specific interaction between the virus and a receptor on the cell surface (2,5,6). The viral receptor-finding process is central because it determines the targeted cell types through virus-receptor specificity. Furthermore, viral binding to receptors or co-receptors may modulate subsequent steps of the infection process by inducing reorganization of the lipid membrane and the cytoskeleton, thereby affecting the mechanism of viral genomic delivery and pathogenesis (1,4,6).

In mammalian cells, the binding of a virus to the cell surface may involve nonspecific weak interactions with co-receptors for concentrating viruses on the cell surface (2), followed by specific interactions with receptors facilitating cellular delivery of the viral genome (2,3,6). It has been shown that an effective concentration of receptors at the immediate vicinity of the virus is required to promote irreversible attachment and viral genomic delivery (2,4,7). Single virus tracking studies on live cells and supported lipid bilayers indicated that the mobility and confined localization of viruses and virus-receptor complexes depend on the lipid environment, cortical actin network, and receptor aggregation in nanometer-sized domains (8,9). Although these findings offer some insights into the early stages of virus-host interaction, a quantitative understanding of the spatiotemporal dynamics that underlie virus-receptor

finding is still lacking, even for the simplest systems. In particular, the dependence of viral target-finding on virus-receptor interactions and cellular architecture remains unclear. Here we address these issues with the use of a virus-host model system.

The *Escherichia coli* bacterium and its virus, bacteriophage λ, are a well-established virus-host model system (10–12). Phage λ hijacks the bacterial maltose pore LamB (λ-receptor) for delivery of its genome into the bacterial cell (11–15). The interaction between phage λ and its receptor has been extensively studied both at the molecular level (14,16) and in bulk (11–13,17). The results of these studies suggest that the rate of phage absorption onto the host cells is extremely high, possibly exceeding the theoretical value based on diffusion-limited kinetics (11,12). A recent study indicated that the early viral infection process in the λ-system proceeds in two steps: an initial reversible virus-host association, followed by irreversible attachment (13). The LamB receptors on the host cell were found to be required for both reversible and irreversible virus-host associations. Another study showed that infecting λ phages and other viruses bind preferentially to the bacterial poles (17). Although the mechanism of viral target finding in this system is unknown, these reports provide a starting point for further investigation of the search process, and may offer insights into target finding processes in higher systems.

Here we applied real-time single-particle tracking of individual fluorescent viruses on live cells to obtain viral trajectories with nanometer accuracy (18). Viral trajectories displayed nonisotropic motion patterns on cells, and a unique spatial localization along the cells, even before binding occurred. These features were correlated with the

spatial organization of the receptor network. Additionally, virus-receptor colocalization and analysis of trajectories on receptor-deficient cells indicate that the viral receptor-finding process is governed by a weak interaction with the network of receptors. We used our quantitative spatiotemporal data to derive a theoretical model of the target-finding process, which enabled us to reproduce the experimental spatial focusing phenotype as well as other features of phage dynamics.

MATERIALS AND METHODS

Bacterial strains and growth conditions

Strain LE392 (genotype: *sup*F), was used as the wild-type host. The S2188 strain (deleted LamB gene) harboring the pLO16 plasmid was used for production of biotinylated LamB (bio-LamB) receptors [19]. The same strain without the plasmid was used as a control for the virus-host interaction in the absence of LamB receptors.

An overnight culture of indicator strain LE392 was diluted 1:100 in Luria-Bertani (LB) broth containing 0.2% (w/v) maltose and 10 mM $MgSO_4$, and grown at 37°C to $OD_{600} \approx 0.4$ (measured using SmartSpec Plus; Bio-Rad). The cells were centrifuged at $1000 \times g$ for 10 min at 4°C in an Eppendorf centrifuge (model 5804R) and the pellet was gently resuspended in 1/10th of the original volume in 10 mM $MgSO_4$.

Fluorescent phage

The fluorescent phage λ_{LZ1} [20] is gpD-EYFP, *cI*857 *Sam*7 *D-eyfp b::kan^R*. An overnight culture of lysogen LE392(λ_{LZ1}) was grown in LBM medium (LB + 10mM $MgSO_4$) in the presence of appropriate antibiotics. The culture was diluted 1:100 into LBM and grown at 30°C with mild shaking (180 rpm) to $OD_{600} \approx 0.5$. The lysogen culture was induced by increasing the temperature to 42°C for 15 min, and then incubated at 37°C with mild shaking until lysis was visible (i.e., the culture became clear). After addition of 2% chloroform (Fisher Scientific), the culture was incubated for 15 min at room temperature (~25°C). The culture was centrifuged (at $4500 \times g$ for 10 min at 4°C in an Eppendorf centrifuge (model 5804R)) and the supernatant was recovered. The sample was further concentrated (~1/5 of initial volume) with the use of an Amicon Ultra-4 centrifugal filter unit with an Ultracel-50 membrane (Millipore) and centrifuged at $4500 \times g$ for 5 min.

Infection setup

Glass coverslips and slides were cleaned (20 min of sonication with 1 M KOH followed by 5 min of plasma cleaning). The coverslips were precoated with poly-L-Lysine (No. P8920; Sigma) for cell attachment. Perfusion chambers were assembled with the use of double adhesive tape (serving as a spacer) and sealed with epoxy. Cells (20 μL) were added to the perfusion chamber through a predrilled hole. After 5 min of incubation, the perfusion sample was washed with 200 μL of PBSM buffer (PBS buffer + 10mM $MgSO_4$) to remove excess cells. The chamber was placed under the microscope to verify sufficient attachment of cells to the surface, followed by the addition of fluorescent viruses in infection buffer (20 μL; see Movie S1 in the Supporting Material).

Labeling of LamB receptors

An overnight culture of S2188:pLO16 was diluted 1:200 in LB with addition of the appropriate antibiotics. Cells were grown until they reached the log phase (OD_{600}~0.3), whereupon isopropyl-β-D-thio-galactoside (IPTG) was added to induce LamB receptor production. The cells were grown for another

45 min (reaching $OD_{600} \sim 0.5$) before they were harvested, and then centrifuged at $1000 \times g$, 4°C, for 10 min. The supernatant was discarded and the cell pellet was resuspended in 1 mL PBSM buffer. The bio-LamB receptors were specifically labeled with streptavidin (SA)-conjugated fluorophores (SA-Atto565 (Fluka) and SA-Qdot 655 catalog No. Q10121MP; Invitrogen). SA-Qdot 655 was selected as the fluorophore of choice because of its superior photostability and emission intensity. For labeling, SA-conjugated fluorophores were added to 100 μL of PBSM-resuspended cells. Different concentrations of SA-conjugated fluorophores were added to the cells to visualize different features of the LamB receptors. To distinguish individual receptors for single receptor tracking, a concentration of 10–100 pM SA-conjugated fluorophores was used. To visualize the arrangement of the LamB receptor network, a concentration of 1–10 nM was used.

After addition of the SA-conjugated fluorophores, the cells were mixed by pipetting and stored at 4°C for 30 min. To separate labeled cells from free fluorophores, 400 μL PBSM was added to a total volume of 500 μL and the solution was mixed by pipetting. The cells were centrifuged at $1000 \times g$ for 5 min at 4°C. The supernatant was discarded and the cell pellet was gently resuspended in 500 μL of PBSM. Centrifugation and resuspension were repeated four times, and then the cells were finally resuspended in 50 μL of PBSM for imaging.

Microscopy

To track individual viruses and image single receptors and the receptor network, the sample was mounted on an Olympus microscope (IX70) with an oil immersion objective (100× NA 1.4). The 488-nm line of an air-cooled Ar-ion laser was used in highly inclined, total internal reflection excitation of fluorescence from both quantum dots (QDs) and EYFP phages. The fluorescence was separated via a dichroic mirror and the appropriate emission filters, and imaged with a high quantum efficiency, charge-coupled device (CCD) camera (Andor Ixon+ true EM gain camera). The CCD exposure was set to 33 ms at high gain, with a minimum of 1000 images captured for each movie.

Imaging cells with labeled LamB

For imaging, 1 μL of the labeled cells was diluted 1:10 into PBSM at room temperature and placed on a thin 1.5% LBM-agarose slab (~1 mm thick). After 1 min, a coverslip (No. 1; Fisher Scientific) was gently overlaid and the sample was imaged under the fluorescence microscope at room temperature. Microscopy was performed on an inverted epifluorescence microscope (Eclipse TE2000-E; Nikon) with a 100× objective (Plan Fluo, numerical aperture 1.40, oil immersion) and standard filter set. Images were acquired with a cooled CCD camera (Cascade512; Photometrics). Acquisition was performed with the use of MetaMorph software (Molecular Devices).

To create a three-dimensional (3D) reconstruction of the LamB network, labeled cells were imaged in a series of 31 images along the *z* axis with 50 nm spacing. Receptors were recognized by using thresholding routines implemented in the MATLAB image-processing toolbox (The MathWorks, Natick, MA). The resulting binary images were stacked to form 3D representations of the LamB network. This showed a helical pattern that was well represented by two helices out of phase, or a single helix that was continuous through the pole (see Fig. 2 *B* and Movie S2).

For full details regarding the materials and methods used, including data analysis and theoretical calculations, see the Supporting Material.

RESULTS

Tracking individual viruses during infection

We examined the receptor-finding process at the single-virus, single-cell level by using a modified λ-strain with

a fused fluorescence protein (EYFP) [19]. To follow the infection process, we attached live *E. coli* cells to the coverslip of a microfluidic chamber and then added the fluorescent viruses (detectable as diffraction-limited spots; see Fig. S1 and Movie S1). Fig. 1 *A* shows a sequence of images (30 ms exposure time per image) in which a diffusing virus (*green*) approaches a cell (*black*) and finally attaches to its surface. We analyzed the movies using a FIONA [18] algorithm, yielding the peak position and fit accuracy of the viral trajectories projected in two dimensions, and plotted on the corresponding cells' outline for analysis in a cellular frame of reference (see Supporting Material and Fig. S2).

The trajectories showed three different modes of motion: free diffusion, motion on the surface of the host cells, and attachment (see Fig. 1, *A* and *B*). The different modes of motion exhibited at least an order of magnitude difference

in the instantaneous velocity, discerned within individual trajectories (Fig. 1 *C*). To characterize the different modes of motion, we calculated the mean-square displacement (MSD) $\delta^2(\tau)$ of the trajectories in each motion regime, where $\delta = |\mathbf{r}(t + \tau) - \mathbf{r}(t)|$ is the displacement between two time points, and δ^2 is averaged over all pairs of time points with difference τ between them [21]. The MSD plots in Fig. 1 *D* clearly show three distinct motion regimes. Both free viruses off-cells and viruses moving on the cell surface exhibited normal (Fickian) diffusion ($\delta^2 \approx D\tau^\alpha$, with the exponent α close to one ($\alpha = 0.98 \pm 0.2$ and 1.1 ± 0.1 for 35 and 72 trajectories, respectively)), but with an order of magnitude difference in the diffusion coefficient D. Viruses that were attached to the cells exhibited slow local motion, with possibly subdiffusive characteristics ($\alpha \sim 0$–0.5, with a mean of 0.3 ± 0.2 for 120 trajectories) [21].
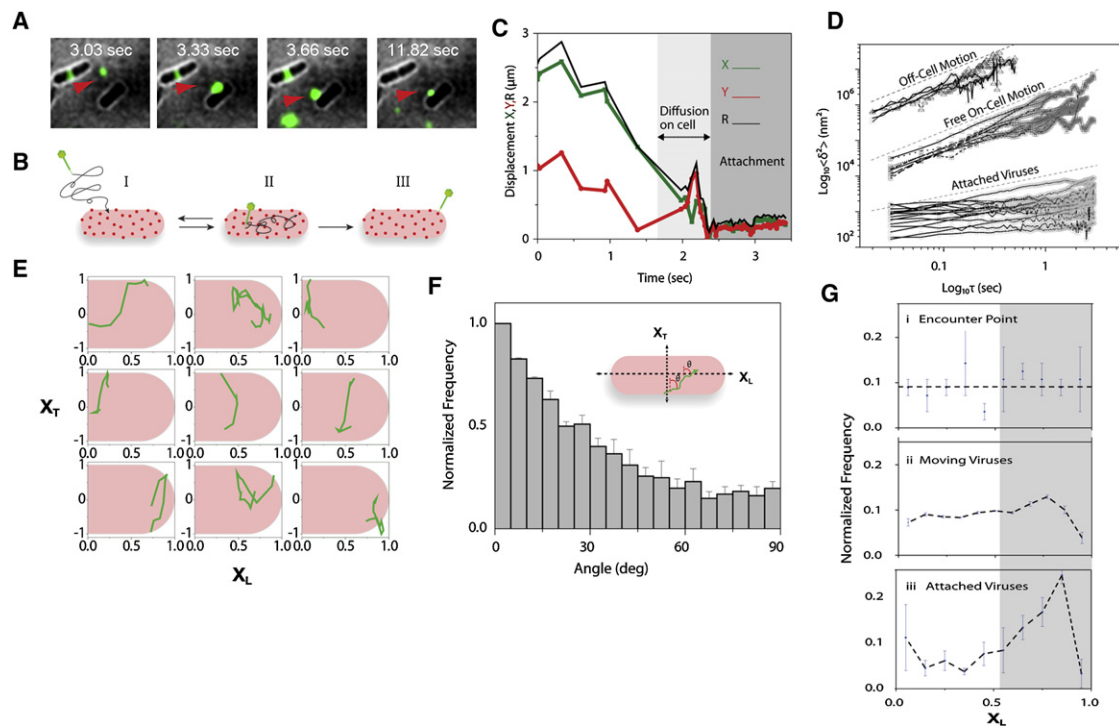

FIGURE 1 Tracking the target-finding process of individual viruses. (*A*) Time-lapse images of a single fluorescent λ-phage virus (*green spot*, indicated with a *red arrow*) diffusing near and on an *E. coli* host cell (*black*) until it attaches to a receptor (cropped images scale: height = 10 μm, width = 11 μm). (*B*) Illustration of the observed stages for the virus receptor-finding process: (*I*) The virus initially diffuses freely until it encounters a cell, followed by (*II*) motion on the host cell and (*III*) binding to a receptor (or detachment from the host cell and continued free diffusion). (*C*) Trajectory of a single virus starting at free 3D motion followed by diffusion on the cell and attachment. The displacement in both *X* and *Y* coordinates (*green* and *red*, respectively), and the total displacement R (*black curve*) are shown. The transitions between off-cell diffusion, on-cell motion, and attachment are marked. (*D*) The calculated MSD as a function of lag time for individual viral trajectories in each of the observed regimes, forming distinct groups with more than an order of magnitude separation in MSD values: off-cell diffusion trajectories (*top group*), on-cell diffusion (*middle group*), and attachment (*bottom*). Trajectories for both off-cell diffusion and on-cell diffusion yielded a log-log slope of ~1 (see text), indicative of normal diffusion. Viruses bound to the host showed either small, confined movement or no movement, with a 0.5–0 slope range (see text). (*E*) Nine representative single-virus trajectories plotted in normalized bacterial coordinates (X_L, long axis; X_T, short axis; see Fig. S2), showing a tendency for motion along the short axis X_T (perpendicular to the long axis). (*F*) Normalized distribution of the angle between the momentary displacement vector and the short axis, X_T, calculated for 138 viral trajectories (see Supporting Material). The histogram shows a predominant inclination for motion along the short axis (X_T) with a mean angle = $29.6 \pm 0.4°$ (mean $\pm$ SE, SD = 24.38 degrees). (*G*) Distributions of virus positions along the cell (X_L) throughout the spatial focusing process. Error bars: mean $\pm$ SE. (*i*) Initial random point of encounter (from 47 viral trajectories). (*ii*) Trajectories of unbound viruses moving on the surface of the host, showing an affinity for the pole (from 138 viral trajectories). (*iii*) Distribution of final infection sites with a clear trend for polar localization (from 59 viral trajectories). The area of all three distributions was normalized (summed frequency = 1; see Supporting Material) to facilitate comparison between the different distributions.

Anisotropic viral trajectories and the spatial focusing process

To characterize the viral search process, we focused on viral motion that occurs on the surface of cells before attachment/detachment takes place. The viral trajectories were represented in a normalized two-dimensional (2D) coordinate system, along (X_L) and across (X_T) the host cell (see Fig. S2). This representation enabled us to correlate the viral trajectories with the geometry of the host cells, and to unveil universal spatial features in the behavior of many individual viruses. We first observed that the trajectories of viruses exhibited a distinctly anisotropic motion pattern, tending to move along X_T (Fig. 1 E). To quantify this phenomenon, we measured the absolute value of the angle of the instantaneous velocity vector relative to X_T, where the angle distribution from 138 trajectories (Fig. 1 F) yielded a mean motion angle of $29.6 \pm 0.4°$ (error bars: mean $\pm$ SE).

The viral trajectories on the cell surface were also found to be inhomogeneous (Fig. 1 G), exhibiting a spatial focusing along the cell. The initial virus-host points of encounter were uniformly distributed (Fig. 1 G-i). However, subsequent virus trajectories showed an affinity to reside in specific regions along X_L, including the cellular pole (Fig. 1 G-ii and Fig. S2). Finally, the bound viruses were spatially focused and showed a distinct preference for the cellular poles (Fig. 1 G-iii). No localization trend was observed along X_T (see Fig. S3).

Organization of the LamB receptor network

The observed tendency of viral motion to traverse the cell, as well as the focusing of viral positions, led us to ask whether these features reflect an interaction with an ordered pattern on the surface of the cell, specifically with the viral receptors, LamB. Previous studies (22) using fluorescently labeled λ phage tails revealed a spatial arrangement of LamB receptors on the E. coli surface that was reminiscent of the helices and rings found for other bacterial surface proteins (23,24). To examine the arrangement of LamB receptors on the cell surface, we used an E. coli strain (S2188:pLO16) with an inducible expression for a modified version of the LamB protein that is biotinylated at low efficiency in vivo (25), which enabled specific labeling using SA-conjugated fluorophores.

We first labeled cells using a low concentration (100 pM) of SA-QDs to track individual receptors (Fig. 2 A, left panels). We found that the receptors were either immobile or exhibited slow, confined motion comparable to that of attached viruses (Fig. S5 and Fig. S6, respectively). Labeling multiple receptors with a high concentration of QDs (10 nM) enabled us to characterize the spatial organization of LamB on the cell surface. Fig. 2 A (right panels) shows representative images of highly labeled cells, in which various striped patterns reminiscent of rings and helices can be observed (see also Fig. S7). Fig. 2 B shows a 3D-rendered image of a highly labeled cell obtained
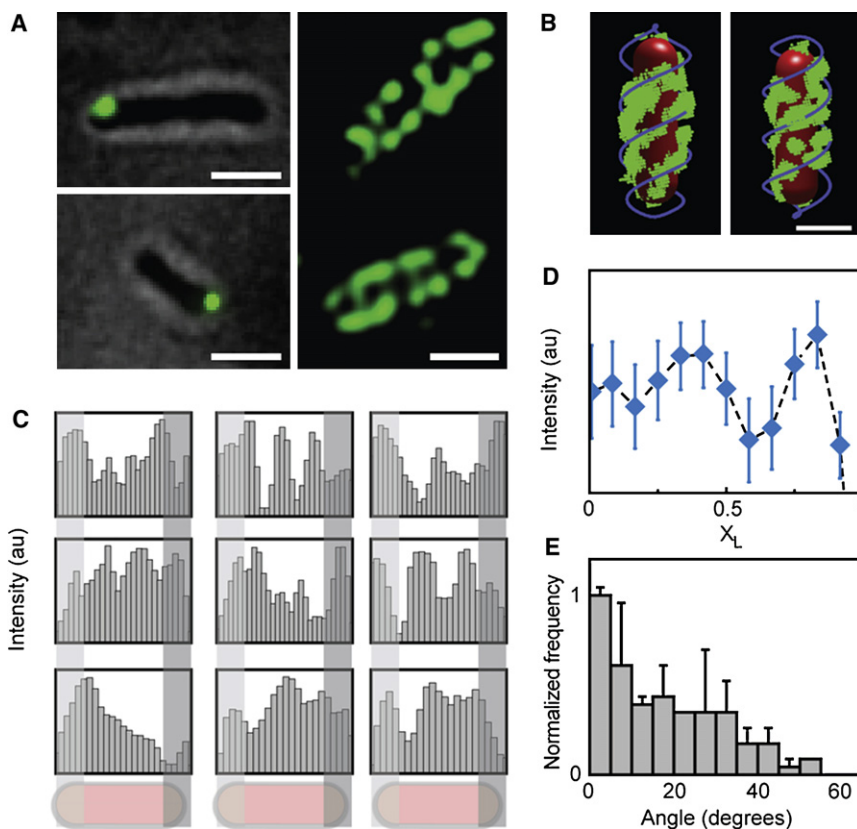

FIGURE 2 Arrangement of the LamB receptors network. (A) Labeling of bio-LamB receptors with SA-conjugated 655 Qdot. Left panels: At a low concentration of QDs (100 pM), single receptors are labeled (green spots) and their motion on the cells (gray) is tracked. Right panel: Increasing the concentration of QDs (5–10 nM) provides extensive labeling of bio-LamB receptors, allowing the organization of the LamB receptor network (green bands) into bands, rings, and helices, and combinations thereof to be visualized (scale bar = 2 μm). (B) Rendered 3D image obtained by sectioning epifluorescence microscopy of cells with labeled receptors, showing nearly continuous helices (scale bar = 2 μm). (C) Distribution of the LamB receptors along nine individual E. coli cells. The distribution of fluorescence intensity along the cells length shows peaks consisting of the various LamB bands (rings and helices). Distinct peaks at the poles are observed in most cells. (D) Normalized (per cell) LamB distribution along X_L averaged for 50 cells, showing a clear peak at the cellular poles indicative of a high concentration of receptors. (E) Angular distribution of LamB bands from 98 cells, showing a tendency for band orientation along the short axis X_T (perpendicular to the long axis).

through sectioning, which is suggestive of a continuous helix (see also Movie S2).

We analyzed images of highly labeled cells to extract the spatial characteristics of the LamB network. The distribution of receptors along individual cells showed distinct peaks corresponding to the observed rings and helices (Fig. 2 C). An analysis of the weighted average of fluorescence profiles from 50 cells (Fig. 2 D) revealed a unique region with high receptor concentration around the cell pole. LamB bands (98 cells; Fig. 2 E) displayed a preference for alignment along the short axis of the cell (mean angle = 23.8 ± 1.9°; error bars: mean + SE).

The organization of the LamB receptors shows a striking resemblance to features exhibited by viruses moving on the cell surface, including 1), a similar angular distribution for viral trajectories and LamB bands (compare Figs. 1 F and 2 E); and 2), increased viral affinity for polar localization (Fig. 1 G) and distinct LamB bands at poles (Fig. 2 D). These similarities suggest a unique virus-receptor interaction resulting in an increased viral residence in receptor-rich regions.

Probing the virus-receptor interaction

To test whether viral motion is indeed governed by interaction with LamB receptors, we compared the dwell times of viruses on wild-type cells and receptor-deleted cells (Fig. 3 A) (25,26). Cells lacking receptors exhibited a >15-fold decrease in dwell time, suggesting that LamB

receptors are required for prolonged interaction between viruses and cell surface. The importance of the virus-receptor interaction was further highlighted by the phages' motion (Fig. 3 B and Table S1), in which case the 3D instantaneous diffusion coefficient was similar to the diffusion coefficient on cells lacking receptors. Meanwhile, the diffusion coefficient of attached viruses was very close to that of individual receptors. Finally, the diffusion coefficient of viruses moving on cells expressing LamB had an intermediate value.

To further confirm that viruses moving on cells interact primarily with the LamB receptors, we examined the colocalization of moving viruses and receptors. Fig. 3 C shows time-lapse images of a virus (green) moving on a cell (blue) with labeled LamB receptors (purple; see also Fig. S10). An analysis of viral trajectories showed that the viruses spent a mean of 73.6 ± 3.7% of their total trajectory time in receptor-rich regions (Fig. 3 D, for 70 labeled cells). This value constitutes a significant oversampling of the receptor (labeled) regions, whose average coverage of the cell surface was 57.6 ± 1.5% (Fig. 3 D, inset), attesting that viral motion is governed by interaction with LamB receptors.

Theoretical model for viral target finding

To consolidate and test our quantitative understanding of the viral receptor-finding process, we formulated a theoretical model of the underlying dynamics. We extracted the
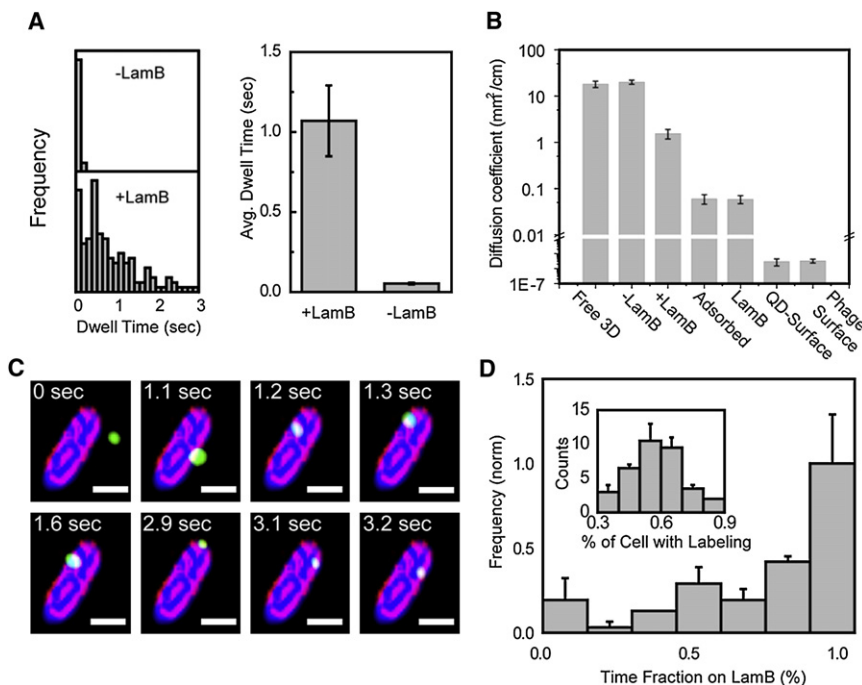

FIGURE 3 Viral motion on the cell surface is dominated by the interaction with LamB receptors. (A) Left panels: Distribution of dwell times of viruses on host cells with and without LamB (+LamB and –LamB, respectively). Right panel: The resulting mean dwell times, showing a major reduction in viral on-cell dwell time on the cells lacking LamB. (B) The instantaneous diffusion coefficient (see Supporting Material) of viral motion extracted from individual trajectories (Table S1). The Off-cell diffusion and diffusion on a LamB-deleted host (−LamB) resulted in a similar diffusion coefficient; however, diffusion on the host with LamB (+LamB) was slowed compared with the former. Diffusion of attached viruses and diffusion of individual LamB receptors labeled with QDs also resulted in similar values, indicating that attached phages are indeed bound to receptors. Controls: QDs tethered to the surface, and viruses adsorbed to the surface (error bars: mean ± SE). (C) Time-lapse images of the colocalization of a free virus (green) moving on a cell (blue) with highly labeled bio-LamB receptor bands (purple). The virus is observed to be predominantly moving on the LamB receptor bands (scale bar = 2 μm). (D) Colocalization dwell-time analysis of 70 unbound viruses moving on cells with labeled bio-LamB, showing the distribution of the fraction of a trajectory the viruses spent on LamB regions, with strong prevalence for residing in highly labeled, receptor-rich regions. Inset: Distribution of the cell area (fraction of entire area) with labeled receptors.

relevant physiological and kinetic parameters from experimental data, and calculated the model using stochastic simulations (Fig. 4; see Supporting Material). *E. coli* cells were modeled as cylinders with spherical caps. For each cell, the cell size defined the pitch of a double helix according to the relationship obtained experimentally (Fig. S8). This double helix was defined as a receptor-rich area, and the remainder of the cell surface was defined as receptor-free. Viral motion on the cell surface obeyed the following rules: A virus located in a receptor-rich zone may move randomly (diffuse) within the receptor-rich area, it may become attached to the surface, or it may move into a receptor-free area. A virus located in the receptor-free area may diffuse within this area, diffuse into the receptor-rich area, or fall off the cell surface.

We simulated the motion of 10,000 viruses using an algorithm for curved surface diffusion (21,27). The resulting trajectories exhibited the spatial focusing feature seen in experiments (Fig. 4 *E*), i.e., viruses arriving at random places along the cell (*top curve*) gradually concentrate at receptor-rich regions (*middle curve*). The final attachment sites show a pronounced preference for the receptor-rich areas, and especially the cell poles (*bottom curve*). Thus, the simple assumptions invoked in our model (i.e., differences in movement, attachment, and falling-off probabilities between two regions in the cell) combined with experimentally extracted kinetic parameters are sufficient to reproduce the observed phenomenology of the target-finding process.

DISCUSSION

Target-finding in the phage λ system

Our observations led us to conclude that the virus-host interaction is predominantly mediated by the host's LamB receptors (14,16) through two types of interactions: First, a weak and reversible receptor-sampling interaction stalls viruses in receptor-rich regions and slows their diffusion (Fig. 3, *B* and *C*). Second, as a consequence of the preliminary receptor-sampling interaction, the virus locks onto a receptor in a strong and irreversible receptor-binding interaction. The sampling interaction will dominate the receptor-finding process (Fig. 1 *G*) because viruses will sample more and reside longer in receptor-rich regions. Consequently, the probability of binding a receptor will be higher in highly sampled regions, which are nonuniformly distributed along the cell, resulting in spatial concentration of viruses and the observed spatial-focusing behavior. Therefore, the receptors' spatial organization (ring and helices) and distribution (density along those regions) may be advantageous for the viral search process because they lead to increased sampling in those regions. In an alternative scenario in which receptors are uniformly distributed, the low sampling rate would result in a significantly lower receptor-binding probability.

Target-finding as a reduction-of-dimensionality process

Beyond the specifics of the phage system, our findings may provide broad insights into target-finding processes in biology. The kinetics of molecular binding to cell surface receptors has been the topic of numerous studies. In a pioneering work, Adam and Delbruck (28) introduced the concept of rate enhancement by the reduction of dimensionality. They proposed a two-stage capture process, with a transition from 3D diffusion in bulk to 2D diffusion on the surface of the cell, resulting in increased target-finding rates. Berg and Purcell (15) provided an additional analysis for the two-step capture process and explicitly calculated the expected kinetics for λ-binding. Discrepancies between their calculations and the experimental results obtained by Schwartz (11,12) were attributed to bacterial swimming. Later studies incorporated the effects of reversible binding to the cell surface (29). The two-step capture process we observed may also represent a dimension-reduction scheme, albeit a different from the one previously envisioned (11,12,15,28,29). The interaction of viruses with a network of receptors on the cell surface limits their sampling motion to a fraction of the surface, in effect rendering it quasi-one-dimensional, or possibly of a fractal dimension between 1 and 2. Thus, the reduction in dimensionality in the transition from bulk (3D) to cell surface is larger than previously assumed. This new (to our knowledge) insight may enhance our understanding of the target-finding process and may possibly clarify previous inconsistencies between theoretical models and experimental observations (11,12,15,28,29).

Implications for other virus-host systems

Finally, it is interesting to speculate on the possible implications of our findings in the context of early virus-host interactions in higher systems. Obviously, such systems exhibit complex and varied phenotypes with regard to cell-surface attachment, target receptors, and delivery and propagation pathways (1,3,4,6). Nevertheless, some features in common with our simple model system should be noted: The initial binding to the surface of host cells typically occurs through a nonspecific weak interaction with attachment groups, or co-receptors, and is followed by a more specific interaction with the primary receptors (1,2,6). The binding to both attachment factors and viral receptors is typically weak and reversible, and strong binding requires simultaneous attachment to a number of receptors and hence an increased local density of receptors (1–6). These common features may suggest a universal virus-host search process. It has been shown that the motion and binding of viruses depends on the local lipid environment and actin network, indicating a correlation between skeletal factors and concentration of receptors, possibly governing the search and target-finding
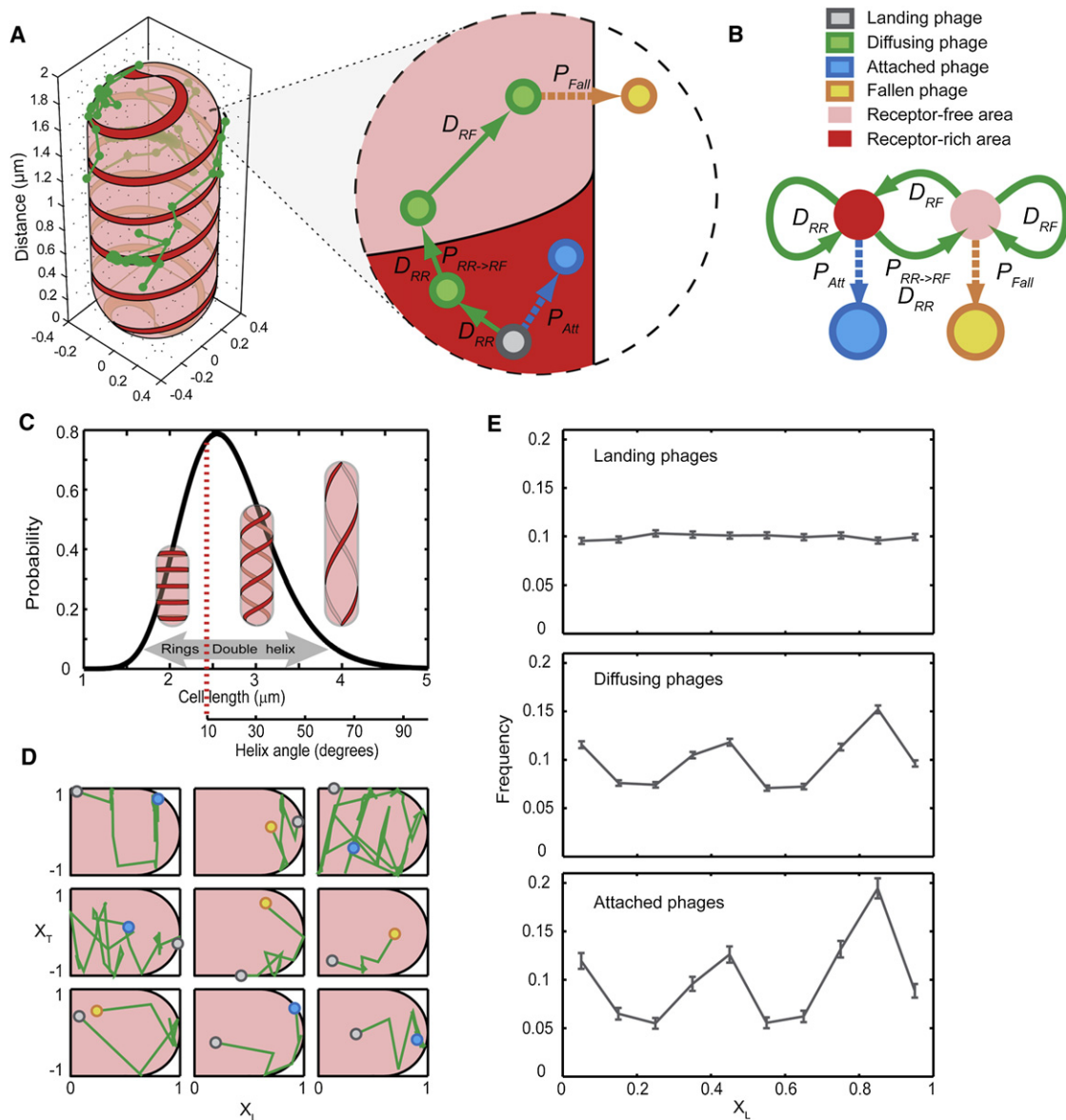
FIGURE 4 Theoretical model of phage target finding. (*A*) A schematic description of the model, showing a typical phage trajectory (*green*) on the surface of an *E. coli* cell. Cell shape was modeled as a cylinder with hemispherical caps (radius $R_c = 0.4$ μm). The cell surface was divided into receptor-free (*transparent pink*) and receptor-rich (*solid red*) areas. The receptors form a 50-nm-thick double helical or multi-ring pattern along the cell surface. The zoomed-in area shows the kinetic scheme in detail. A phage located in a receptor-rich zone can either move within the receptor area with a stepsize consistent with the diffusion coefficient D_{RR}, become attached with a probability P_{Att} (chosen to match the experimentally observed dwell time to attachment), or move into a receptor-free zone. This move can be rejected with a probability $1 - P_{NR \rightarrow R}$, in which case the move will be repeated. On the other hand, a phage located in a receptor-free area can move with a diffusion coefficient D_{NR}. If the phage attempts to enter the receptor zone, the move will always be allowed. The phage can also fall off the cell with a probability $P_{Fall} = \tau_{sim}/\langle\tau_{Fall}\rangle$, where τ_{sim} is the time step of the simulation and $\langle\tau_{Fall}\rangle$ is the experimentally observed dwell time to fall-off in a LamB- *E. coli* strain. (*B*) A simplified kinetic scheme of the model, shown as a four-state, discrete-time Markov chain. The nonreceptor (NR) and receptor (R) states are transient, and the attachment (A) and fall-off (F) states are absorbing. (*C*) Generating population heterogeneity. Cell lengths were randomly chosen from a log-normal distribution spanning the experimentally observed cell sizes (Fig. S5). The cell size defines the pitch of receptor double helix according to the relationship obtained experimentally. For short cells with helix angles of <10°, a multi-ring pattern was used instead of a double helix. (*D*) Representative 2D projections of phage trajectories in normalized units (*green lines*). The initial landing site is shown as a gray circle. Panels in the first two rows display trajectories ending in attachment (*blue circle*), and panels in the last two rows display trajectories ending with the phage falling off the cell (at a position denoted with a *yellow circle*). (*E*) Histograms of phage position along the long axis of the cell (in normalized units; 0 corresponds to the cell center, and 1 is the cell pole). The lines correspond to the distribution of landing sites (*top panel*), diffusion trajectories (*middle panel*), and attachment sites (*bottom panel*). A gradual focusing effect can be observed whereby the phages begin at a uniformly distributed landing site but end up with a nonuniform distribution, enriched at the cell pole. Error bars are the mean ± SE from 10,000 independent trajectories.

pathways in a similar spatial focusing manner ([4,8,9,30]). Further studies of early virus-host interactions in other systems may enable us to identify a universal viral target-finding process.

SUPPORTING MATERIAL

Materials and methods, single-virus target finding assay, data analysis, theoretical model, three tables, references, 11 figures, and two movies are available at http://www.biophysj.org/biophysj/supplemental/S0006-3495(11)00584-4.

REFERENCES

1. Dimitrov, D. S. 2004. Virus entry: molecular mechanisms and biomedical applications. *Nat. Rev. Microbiol.* 2:109–122.

2. Marsh, M., and A. Helenius. 2006. Virus entry: open sesame. *Cell.* 124:729–740.

3. Mercer, J., and A. Helenius. 2009. Virus entry by macropinocytosis. *Nat. Cell Biol.* 11:510–520.

4. Skehel, J. J., and D. C. Wiley. 2000. Receptor binding and membrane fusion in virus entry: the influenza hemagglutinin. *Annu. Rev. Biochem.* 69:531–569.

5. Mudhakir, D., and H. Harashima. 2009. Learning from the viral journey: how to enter cells and how to overcome intracellular barriers to reach the nucleus. *AAPS J.* 11:65–77.

6. Smith, A. E., and A. Helenius. 2004. How viruses enter animal cells. *Science.* 304:237–242.

7. Li, E., D. Stupack, …, G. R. Nemerow. 1998. Adenovirus endocytosis requires actin cytoskeleton reorganization mediated by Rho family GTPases. *J. Virol.* 72:8806–8812.

8. Kukura, P., H. Ewers, C. Muller, A. Renn, A. Helenius, and V. Sandoghdar. 2009. High-speed nanoscopic tracking of the position and orientation of a single virus. *Nat. Methods.* 6:923–927.

9. Ewers, H., A. E. Smith, …, A. Helenius. 2005. Single-particle tracking of murine polyoma virus-like particles on live cells and artificial membranes. *Proc. Natl. Acad. Sci. USA.* 102:15110–15115.

10. Lederberg, E. 1950. Lysogenicity in *Escherichia coli* strain K-12. *Microb. Genet. Bull.* 1:5–8.

11. Schwartz, M. 1975. Reversible interaction between coliphage λ and its receptor protein. *J. Mol. Biol.* 99:185–201.

12. Schwartz, M. 1976. The adsorption of coliphage λ to its host: effect of variations in the surface density of receptor and in phage-receptor affinity. *J. Mol. Biol.* 103:521–536.

13. Moldovan, R., E. Chapman-McQuiston, and X. L. Wu. 2007. On kinetics of phage adsorption. *Biophys. J.* 93:303–315.

14. Berkane, E., F. Orlik, …, R. Benz. 2006. Interaction of bacteriophage λ with its cell surface receptor: an in vitro study of binding of the viral tail protein gpJ to LamB (Maltoporin). *Biochemistry.* 45:2708–2720.

15. Berg, H. C., and E. M. Purcell. 1977. Physics of chemoreception. *Biophys. J.* 20:193–219.

16. Wang, J., V. Michel, …, A. Charbit. 1998. Cloning of the J gene of bacteriophage λ, expression and solubilization of the J protein: first in vitro studies on the interactions between J and LamB, its cell surface receptor. *Res. Microbiol.* 149:611–624.

17. Edgar, R., A. Rokney, …, A. B. Oppenheim. 2008. Bacteriophage infection is targeted to cellular poles. *Mol. Microbiol.* 68:1107–1116.

18. Yildiz, A., J. N. Forkey, …, P. R. Selvin. 2003. Myosin V walks hand-over-hand: single fluorophore imaging with 1.5-nm localization. *Science.* 300:2061–2065.

19. Alvarez, L. J., P. Thomen, …, D. Chatenay. 2007. Propagation of fluorescent viruses in growing plaques. *Biotechnol. Bioeng.* 96:615–621.

20. Zeng, L., S. O. Skinner, …, I. Golding. 2010. Decision making at a subcellular level determines the outcome of bacteriophage infection. *Cell.* 141:682–691.

21. Golding, I., and E. C. Cox. 2006. Physical nature of bacterial cytoplasm. *Phys. Rev. Lett.* 96:098102.

22. Gibbs, K. A., D. D. Isaac, …, J. A. Theriot. 2004. Complex spatial distribution and dynamics of an abundant *Escherichia coli* outer membrane protein, LamB. *Mol. Microbiol.* 53:1771–1783.

23. Osborn, M. J., and L. Rothfield. 2007. Cell shape determination in *Escherichia coli*. *Curr. Opin. Microbiol.* 10:606–610.

24. Vats, P., Y. L. Shih, and L. Rothfield. 2009. Assembly of the MreB-associated cytoskeletal ring of Escherichia coli. *Mol. Microbiol.* 72:170–182.

25. Oddershede, L., J. K. Dreyer, …, K. Berg-Sørensen. 2002. The motion of a single molecule, the λ-receptor, in the bacterial outer membrane. *Biophys. J.* 83:3152–3161.

26. Brown, S. 1992. Engineered iron oxide-adhesion mutants of the *Escherichia coli* phage λ receptor. *Proc. Natl. Acad. Sci. USA.* 89:8651–8655.

27. Hołyst, R., D. Plewczyński, …, K. Burdzy. 1999. Diffusion on curved, periodic surfaces. *Phys. Rev. E.* 60:302–307.

28. Adam, G., and M. Delbruck. 1968. Reduction of dimensionality in biological diffusion processes. *In* Structural Chemistry and Molecular Biology. A. Rich and N. Davidson, editors. W.H. Freeman & Company, San Francisco. 198–215.

29. Axelrod, D., and M. D. Wang. 1994. Reduction-of-dimensionality kinetics at reaction-limited cell surface receptors. *Biophys. J.* 66:588–600.

30. Lehmann, M. J., N. M. Sherer, …, W. Mothes. 2005. Actin- and myosin-driven movement of viruses along filopodia precedes their entry into cells. *J. Cell Biol.* 170:317–325.